Effect of thermo-mechanical ageing on materials and interface properties in flexible microelectronic devices

Anthony Chapel, Jérôme Fortineau, Nicolas Porcher, Simon Malandain, Séverine Boucaud-Gauchet

Article

Effect of thermo-mechanical ageing on materials and interface properties in flexible microelectronic devices

Anthony Chapel [1*], Jérôme Fortineau [1], Nicolas Porcher [2], Simon Malandain [3], Séverine Boucaud Gauchet [1]

[1] Groupe de Recherche en Matériaux, Microélectronique, Acoustique et Nanotechnologies (GREMAN), UMR-CNRS 7347, INSA Centre Val de Loire, Université de Tours, 3 rue de la chocolaterie 41000 Blois, France
[2] STMicroelectronics Tours sas 153 rue des Douets 37100 Tours, France
[3] Protavic International Rue du Moulin d'Herbault 37110 Auzouer-en-Touraine, France
* Correspondence: Anthony.chapel@insa-cvl.fr

Received: date; Accepted: date; Published: date

Abstract: The effect of thermal ageing, fatigue and thermo-mechanical ageing on flexible microelectronic devices is studied and reported from a materials and functional durability perspective. The degradation mechanisms of encapsulant and substrate were both studied. Property changes in encapsulant and substrate materials are analyzed and their relationships in the failure mechanisms of the flexible devices determined. Stiffening of the resin under thermal ageing conditions is associated with delamination in test vehicles, which leads to a loss of functional electrical properties. Degradation was due to the prominence of crosslinking reactions occurring during thermal oxidation at 120°C. A moderate stiffening of the resin occurs after fatigue stress testing. Whereas this latter stiffening is similarly associated with crosslinking reactions, here, stiffening could not be induced by thermal degradation of the resin, because the stress frequency employed was low. Instead thermo-mechanical coupling occurred in two stages. Under mild conditions, the degradation mechanisms correspond to the combined effect of thermal ageing and fatigue processes. Under harsher thermo-mechanical conditions, the chain-scission mechanisms become more efficient and induce a softening of the resin.

Keywords: Flexible microelectronics; thermo-mechanical ageing; epoxy resin; durability; encapsulation

1. Introduction

The development of flexible microelectronic devices has led to a blossoming of new applications. Flexible microelectronics allows lightweight and conformable devices to be developed and used as biomedical implants, smart textile, or sensors for the internet of things. Münzenrieder et al developed flexible and stretchable oxide-based electronic sensors for skin and smart-implant uses [1]. Carta et al. designed flexible sensors for monitoring biomedical parameters such as heartbeat, temperature, humidity, and respiratory rate. Most commonly, such sensors were designed and embedded in smart textiles [2].

To achieve such flexibility, however, micro-electronic components have to be interconnected to conformable flexible substrates. Thin, light, conformable, and flexible substrates offer a reliable alternative to rigid printed circuit boards (PCB). Several studies have presented polymers such as polyethylene terephthalate (PET), polyethylene naphthalate (PEN), and polyimide (PI) as suitable candidates to use as flexible substrates [3–5].

Today, the development of flexible, stretchable, and reliable electronic circuits is an important research area. Gonzalez et al. used finite element modeling to determine the geometrical stresses in the metallic connection [6] and arrived at the horseshoe as the optimal geometry. In their review, Rim et al. demonstrated that conductive nanoparticles, deposited via inkjet printing, can offer a suitable solution for processing flexible electronics [3].

Like classical rigid electronic systems, flexible microelectronic devices are susceptible to physical conditions in their working environment. Both electrical circuits and silicon chips are subject to attack by humidity and oxygen from the air. To better prolong the lifetime of these devices, their microelectronic systems require protection by a conformable encapsulant. Here, the encapsulant protects against physical and chemical

attacks from the external environment and mechanical impacts. In particular, it ensures water-tightness of the system[7]. Lewis has outlined the permeability requirement for flexible electronics [8]. Although inorganic encapsulants such as glass readily meet these requirements, they are particularly impractical as flexible devices. Several studies have dealt with the development of flexible encapsulation systems, especially those in the field of organic photovoltaics. For example, Gaume et al. developed an ultra- multilayer barrier based on polyvinyl alcohol (PVA) and clay for such applications [9]. However, the durability of this multi-layer depends on the long-term stability of their composite materials and interfaces. Topolniak et al. studied the ageing of ethylene vinyl alcohol (EVOH)/zeolite composites for the encapsulation of flexible photovoltaics [10] and it was later shown that the photo-oxidation of such composites could lead to a weakening of the barrier properties.

Bossuyt et al. studied the stability of flexible microelectronic devices under cyclic mechanical stretching [11]. They focused on the mechanical cycling effects on the electrical properties of microelectronic devices. Fatigue rupture in electrical copper traces was observable after several hundred thousand cycles.

Although the combined effects of thermal ageing of materials and mechanical stress can occur in many flexible systems and lead to early failure, to our knowledge, only a few papers have dealt with this phenomenon.

In this paper, a flexible epoxy formulation based on ECC and EA is studied as a potential candidate for encapsulation of microelectronic devices. Despite the large number of papers dealing with epoxy resin durability, most have focused on bisphenol A diglycidyl ether (DGEBA) and epoxy amine-based resins [12–15]. Delor-Jestin et al. [14] showed that t the thermal and photochemical stability of DGEBA-based epoxy were both affected by the chemical nature of the curing agent used. Ernault et al. linked the embrittlement of such epoxies upon thermal ageing to changes in their glass transition temperature [13], and β-transitions [12]. The β-transitions are attributable to local motions of hydroxyether groups present in DGEBA [16]. Embrittlement of DGEBA-based epoxy resin is associated with changes in the transitiontemperature and intensity upon oxidative ageing [12].

To be flexible and conformable requires that the chemical structure of the epoxy resins be linear and saturated. Few articles have dealt with saturated epoxy ageing or used mechanical criteria to characterize ageing. Dupuis et al. [17] presented the photo-oxidative degradation mechanism of linseed-based epoxy resin and its effects on the surface and mechanical properties. Their results showed that for shorter irradiation times (<150h), crosslinking reactions induced an increase in nano-hardness, while scission reactions become more competitive at longer irradiations, resulting in a decrease in hardness. The chemical structure of the resin studied mainly consisted of aliphatic chains. In our study, the chemical structure is quite different, with the monomers used based on cyclohexene oxide derivatives. Thus, the main chain segment consisted of a cyclohexane ring linked to an oxygen bridge. The degradation mechanisms also differ from the ones reported in previous publications [14,15].

This paper aimed to identify and understand the destruction mechanisms induced in flexible smartcards by environmental conditions via temperature and mechanical fatigue during their use. The effects of the encapsulant and substrate ageing on the electrical performance and durability of flexible microelectronic devices are presented. This work primarily focused on the polymer material behaviors as the encapsulant and substrate; and the interfacial integrity between the encapsulant/substrate bilayer systems.

2. Materials and Methods

2.1. Materials

The epoxy resin formulation used as encapsulant (named PNE) was developed and supplied by Protavic International. The formulation comprised a mixture of two monomers: 3,4-epoxycyclohexylmethyl-3',4'-epoxy-cyclohexene carboxylate (ECC) and 3,4-epoxycyclohexyl adipate (EA). Their chemical structures are shown in Figure 1. A weight ratio of 1.5 for the ECC monomer to 1 for the EA monomer was employed. Bis[4-(diphenylsulfonio)phenyl]sulfide bis(hexafluoroantimonate) at (0.25-0.50 wt%), also presented in Figure 1, was used as a photo-initiator. The resin was filled with amorphous silicon oxide (30-40 wt%) and cured under UV radiation.

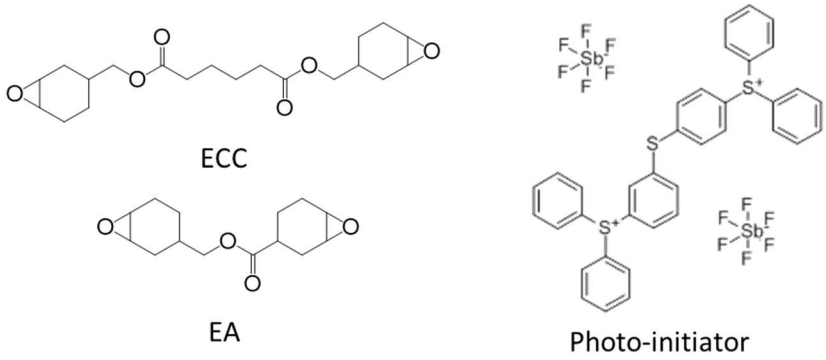

Figure 1. Chemical structures of the two monomers (ECC and EA) constituting the PNE encapsulant and the photo-initiator

2.2. *Sample preparation*

Commercial PET films with a thickness of 120 µm were selected for their flexibility and used as the substrate. A silver electrical circuit was deposited on the substrate and a silicon chip glued to it (Figure 2 a). These systems, called Test Vehicles (TV), were supplied by STMicroelectronics. TVs were encapsulated using a glob top of the PNE resin (Figure 2 b). The glob top architecture, chosen because it advantageously minimizes the amount of protective polymer, also reduced delamination damage by ensuring a lower interfacial surface contact with the substrate. Resin deposition was conducted in a clean room and employed an industrial Asymtek C-341 automatic dispenser. Curing used a 365 nm UV LED for 30 seconds at room temperature under an air atmosphere.

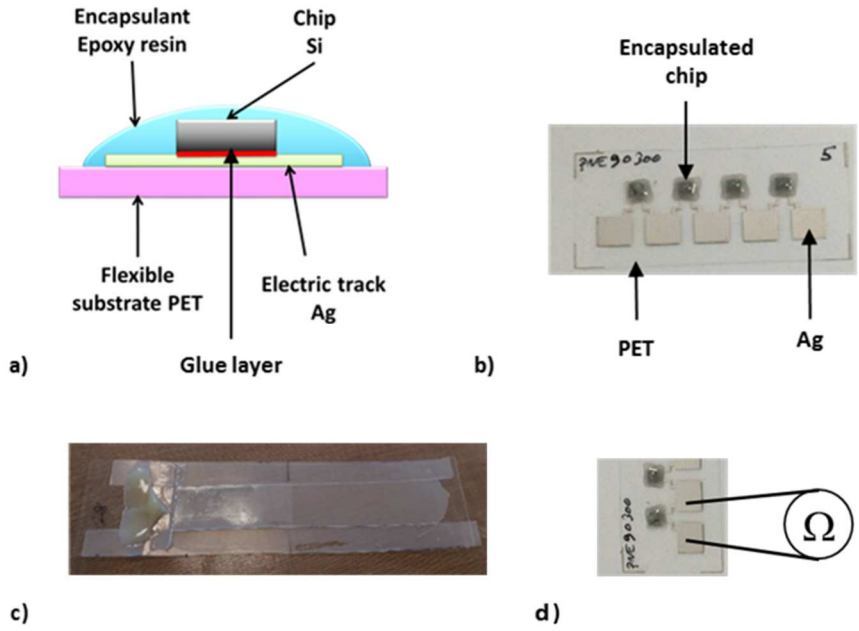

Figure 2. (a) Schematic side view of the glob top encapsulated TV showing the architectural ensemble, (b) TV encapsulated within the PNE resin, (c) multilayered PET and PNE ensemble for the peeling test, and (d) schematic top-view illustrating the experimental assembly of the resistance measurements

Thin 100 µm-thick free-standing epoxy resin films were deposited by bar-coating using an Erichsen Coatmaster model 510 film applicator on a Teflon® sheet. Curing was done in an Eleco model LED Cube 100 UV LED chamber, at a 365 nm wavelength for 90 seconds at room temperature under an air atmosphere.
Multilayer samples were prepared and used to study the interfacial quality of encapsulant/substrate bilayers using the peeling test (Figure 2 c). Epoxy resin films (17 mm width, 100 µm thick) were deposited on PET substrate film (120 µm thick) and cured under the same conditions as the free-standing films.

DSC analysis was employed to verify that the epoxy resin was 100% cured. No residual precursor was detected.

2.3. Ageing conditions

A total of six ageing conditions were performed based on industrial requirements for smartcard applications. Thermal ageing was carried out in a ventilated oven at 120°C for up to 500 hours. Since there is no ageing temperature definition in the ISO10373 standard, the project partner STMicroelectronics proposed conducting thermal ageing at 120°C as recommended for microelectronics devices. This temperature also allowed the simulation of localized heating points that often appear in materials and interfaces during long-term mechanical fatigue tests.

Mechanical fatigue involved the imposition of bending cycles on the test samples by winding them around a roller at a constant frequency of 24 cycles per min, at room temperature. Ageing involved using a homemade bending bench (Figure 3 a). The principle of the mechanical tests is shown in Figure 3 b. Samples were rolled (5 000 cycles) around a 50 mm diameter roller (F1) and then subjected to optical microscopy or electrical testing. If no degradation was noticeable, the samples were again rolled (5 000 cycles) around a 25 mm diameter roller (F2).

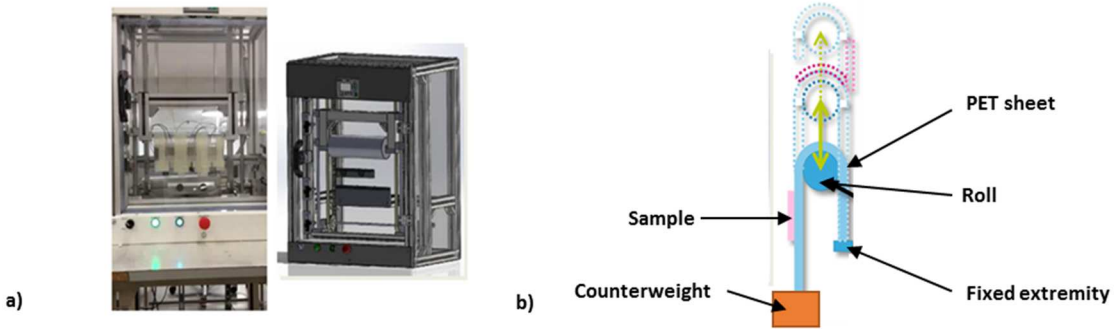

Figure 3. (a) Photograph and (b) schematic illustration of the functional principle of the bending bench

Thermo-mechanical coupling analyses involved subjecting the thermally aged sample to fatigue tests. Samples initially treated for 500 hours at 120°C, were subjected to 5 000 bending cycles around a 50 mm diameter roller (TM1), followed by another 5 000 bending cycles around a 25 mm diameter roller (TM2).

All ageing conditions performed on the samples are reported in **Table 1**. The results presented in this paper were obtained by analyzing up to 7 samples and 4 TVs per condition.

Table 1. Ageing conditions and the number of samples used in this study

AGEING TYPE	**REFERENCE**	**THERMAL**	**FATIGUE**		**THERMO-MECHANICAL**	
CONDITION	Pristine	Up to 500h at 120°C	5000cy ⌀50	5000cy ⌀50 + 5000cy ⌀25	500h 120°C + 5000cy ⌀50	500h 120°C + 5000cy ⌀50 + 5000cy ⌀25
NOTATION	Ref	Xh*	F1	F2	TM1	TM2
Total number of sample	4 TV	4 TV	4 TV	4 TV	4 TV	4 TV
	7 film samples	7 film samples	6 film samples	7 film samples	7 film samples	7 film samples

* X is the ageing time in hours

2.4. Characterization methods

DSC measurements were performed on a Mettler Toledo DSC 1 apparatus under an air atmosphere. Sample masses of 10 mg were placed in aluminum DSC crucibles and subjected to two heating-cooling cycles from 30°C to 250°C at a rate of 10°C/min. DSC analyses allowed us to ascertain curing completion and to monitor changes in the microstructure after ageing. The crystallinity rate (χ_c) for the PET substrate was calculated using a melting enthalpy for 100% crystalline PET of 140 J/g, in line with the literature [18].

Dynamic mechanical thermal analyses were done on a TA Instruments DMA Q800 under air. Rectangular shaped (18 mm x 9 mm) and 100 µm thick samples were analyzed. A tensile dynamic strain of 0.1% was imposed on the samples at a frequency of 1Hz. The samples were heated from -100°C to +100°C at a rate of 3°C/min. The glass transition temperature (Tg) and the β-transition were determined using the loss modulus thermograms. The full width at half maximum (FWHM) of the peaks was also determined.

Tensile tests were carried out on an Instron Microtester 5948 equipped with a 2 kN force cell. Three 100 µm thick rectangular samples (1.7 cm*10 cm) cut from free standing films were analyzed at room temperature, under NF ISO527-3 standard. The preload was 0.5 N and the tensile speed 5 mm.min^{-1}. Three specimen for each ageing condition were analyzed.

Thermo-gravimetric analyses (TGA) were performed on a Setaram Setsys 16/18 apparatus under an air atmosphere. Sample masses of 5 mg were heated from 25°C to 700°C at a rate of 10°C/min. TGA analyses were employed to determine and monitor the degradation temperature corresponding to a mass loss of 5%.

Fourier transform infrared analyses (FTIR) were performed on 20 µm thick films in transmission mode with a JASCO FT/IR-6800 spectrophotometer. FTIR spectra used 32 scan summations at a 4 cm^{-1} resolution.

Determination of epoxy resin adhesion strengths on the PET substrate involved peeling tests performed at a peeling angle of 90° at room temperature. The peeling strengths were directly measured using an Instron Microtester 5948 mechanical testing machine equipped with a 2 kN force cell and a specifically designed peeling bench. The applied load was monitored continuously during epoxy film peeling, at a constant displacement rate of 5 mm/s. The peeling force was determined using:

$$G = F \times (1 - \cos\theta)/w$$

where G is the peeling force (in N/cm), F is the applied load in the stationary domain (in N), θ is the peeling angle (here 90°), and w is the epoxy resin band width (in cm). Three samples for each ageing condition were measured.

Optical microscopy was performed on A Keyence VHX-1000 microscope and employed a 100X optical magnification. The magnification used enabled delamination or formation of cracks to be detected.

Confocal Raman spectroscopy allowed for the in depth chemical structural changes during ageing to be studied. The depth profiles of TV were performed starting from the substrate down to the encapsulating resin. The recorded Raman spectra with an InVia Renishaw microscope used the 633 nm laser line. To allow for analysis of the substrate and then the epoxy resin, samples were placed with the substrate on top. The spectra were recorded at room temperature with various focalizations, from 10 µm for the surface to 200 µm for deep inner sample visualizations at 10 µm intervals.

To detect TV functional failures, electrical tests that involved measuring the electrical resistance between the terminals of the chip (Figure 2 d) were performed. A Fluke 175 true RMS multimeter was used. An increase in the value measured corresponded to device failure and thus defined as the end of life criteria for TV in our study.

3. Results and discussion

3.1. Epoxy resin characterization

Ageing-induced changes of the PNE epoxy resin were determined through thermal and mechanical properties using DMTA, tensile tests and TGA.

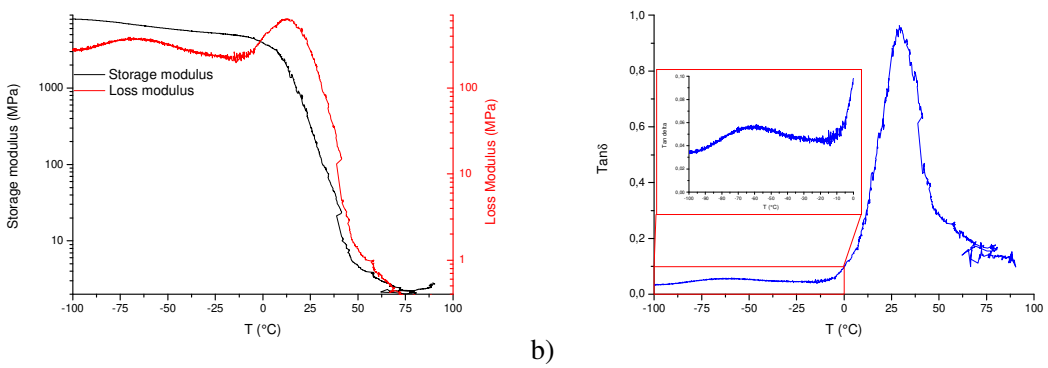

a) b)

Figure 4. DMTA thermograms of unaged PNE epoxy resin showing, (a) storage and loss modulus; and(b) tanδ

DMTA thermograms of the epoxy resin are presented in Figure 4. The main peak of the loss modulus thermogram (Figure 4 a) is centered at +13°C. This peak is attributable to the glass transition of the PNE resin. A secondary maximum at -67°C is attributable to the β-transition of the resin. Udagawa et al. studied the dynamic mechanical properties of UV-cured ECC and EA [19] and attributed the presence of β transition in both polymers to molecular motions of the cyclohexyl rings. As the same chemical structures are present in PNE resin, its β-transition is attributable to the same molecular motions.

Mechanical properties were determined at room temperature using tensile test measurements. Figure 5 a presents a stress-strain curve for the PNE epoxy resin. Epoxy resin films exhibited a brittle break. Both Young's modulus and strain at break were determined. The resin films presented Young's modulus (E) of 33 ± 1 MPa and a strain at break (ε_B) of 22.9 ± 1.1 %.

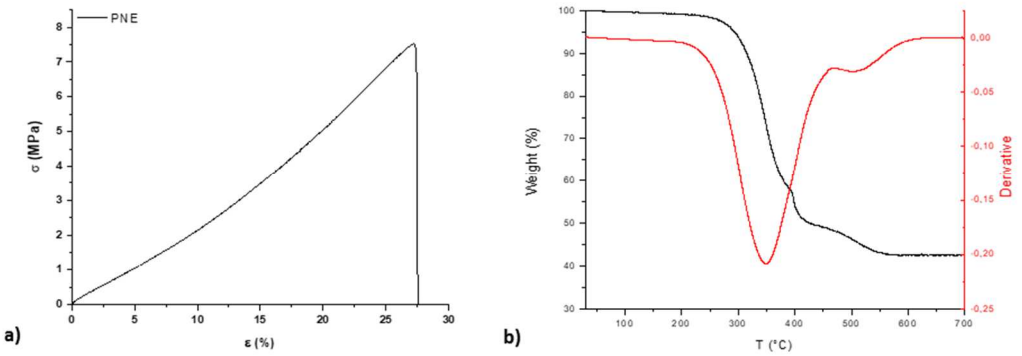

Figure 5. (a) Stress-strain curve and (b) TGA thermogram of unaged PNE resin film

The TGA thermogram of the PNE resin film is presented in **Figure 5** b. Epoxy resin decomposition was at a temperature (T_d) of 294°C. On the derivative curve, two minima were identified at 349°C and at 503°C. Thermal degradation occurred in two stages. At the end of the experiment, 42.5 % of the original weight remained, corresponding to the silicon oxide fillers that do not degrade at these temperatures. Thus, suggesting that the filler content in the studied samples was 42.5 wt%.

3.2. Thermal ageing

Below, the effects of thermal ageing on the encapsulant and the substrate are discussed. Chemical and mechanical analyses for each specimen type are presented.

3.2.1. Epoxy resin ageing

It is important to note that the resin films presented yellowing upon ageing, indicating an alteration of their chemical structure. The evolution of the FTIR spectra with thermal ageing conditions is presented in **Figure 6**. The spectral differences (x hours - reference) in the carbonyl domain (1850-1650 cm^{-1}) are also presented. A white box hides a saturated part of the spectra to facilitate reading. Spectral band formation (upwards) and disappearance (downwards) were detectable on difference spectra.

The main change visible on the original spectra was the decrease in the broad band for wavelengths over 3 000 cm^{-1}. This band is attributed to O-H bonds from adsorbed water or alcohol present in the film. Amid the carbonyl domain, was observed the formation of bands at 1814, 1780 and 1764 cm^{-1}. Whereas the vibration band at 1780 cm^{-1} corresponds to lactones formations [20], the bands at 1814 and 1764 cm^{-1} were attributed to anhydride acids formation.

A decrease in intensity of the band at 1710 cm^{-1} was noticeable. This band signaled the presence of ketones that degrade during thermal ageing.

Although these attributions relied on a reference table and previous literature findings, they should be confirmed by complementary analysis such as chemical derivatization treatments with NH_3 SF_4 or 2,4-dinitrophénylhydrazine (2,4-DNPH) [21,22]. Based on their specific reactivity with the different carbonyl functional groups, these treatments used together with FTIR analysis can identify contributions to the carbonyl band. NH_3 is reactive with esters, carboxylic acids and anhydrides; SF_4 with carboxylic acids; and the 2,4-DNPH with aldehydes and ketones.

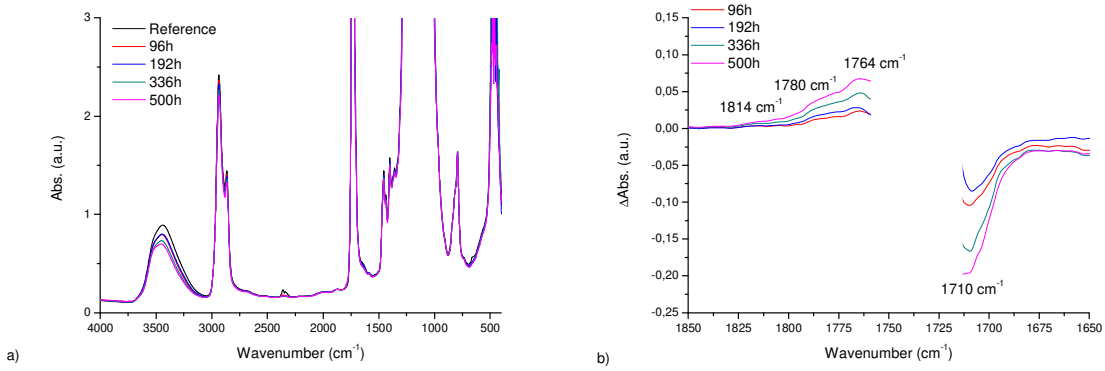

Figure 6. Changes in the epoxy resin films with thermal ageing time (a) full FTIR spectra and (b) FTIR difference (xhours-reference) spectra for the carbonyl domain (1650-1850 cm^{-1})

Table 2 summarizes changes in the thermo-mechanical properties of the resin upon thermal ageing. The Tg and the β-transition were determined using DMTA. The FWHM of the peaks was also calculated. Whereas the Tg increased following thermal ageing, its FWHM remained unchanged. The β-transitions were unaffected by the thermal ageing.

The Young's modulus was four times higher after thermal ageing while the strain at break decreased by a third. This change was well reflected through observed stiffening and embrittlement of the resin films.

The decomposition temperature of the resin increased from 294°C to 307°C.

Table 2. Changes in PNE resin characteristics (T_g, T_β, E, ε_B, T_d) induced by the different ageing conditions

Ageing	T_g	*FWHM of* T_g	T_β	*FWHM of* T_β	*E (MPa)*	ε_B *(%)*	T_d
Reference	13°C	23.1°C	-67°C	36°C	33 ± 1	22.9 ± 1.1	294°C
500h 120°C	26°C	24.2°C	-67°C	38°C	133 ± 32	15.1 ± 1.2	307°C
F1					50 ± 6		
F2	14°C	23.1°C	-71°C	49°C	56 ± 11	15.7 ± 2.2	295°C
TM1	28°C	31.4°C	-67°C	42°C	153 ± 21	17.8 ± 3.7	301°C
TM2	20°C	21.5°C	-69°C	50°C	126 ± 20	20.2 ± 1.0	306°C

Polymer degradation mechanisms in the presence of oxygen involve both crosslinking and chain scissions reactions. These reactions are antagonistic and their kinetics are not identical and can vary according to the degree of degradation, ageing conditions and the nature of the polymer. Crosslinking reactions are usually linked to increases in both Young's modulus and Tg [23,24], whereas chain scission reactions have the opposite effect.

The marked stiffening of the resin studied, coupled with the increase in its glass transition temperature during thermal ageing, could be explained by the dominance of crosslinking reactions over chain scissions in the thermal oxidation mechanism. This result is verifiable by the observed increase in the decomposition temperature, as observed by TGA. It is shown that crosslinking reactions during ageing significantly increase the polymer degradation temperature [25]. Dupuis et al. reported similar result from a study on the photo-degradation mechanism of linseed-based epoxy resin [17]. They showed that crosslinking reactions control degradation for shorter ageing times (200h) and are associated with marked increases in the modulus.

Ernault et al. linked the embrittlement of DGEBA/TTDA and DGEBA/IPDA during thermal-oxidative degradation to crosslinking reactions and β-transition intensity decrease [12]. They attributed intensity decreases in the β-transition to the oxidation of the hydroxypropylether groups of DGEBA since their local motions corresponds to this transition. In the present study, β-transitions for the PNE resin were not affected by thermal ageing at 120°C for 500h. As this transition corresponds to the cyclohexyl ring motions, the molecular mobility of this moiety should be exempt from the thermal-oxidative degradation of the epoxy resin.

3.2.2. PET substrate ageing

To better decipher the events that underpin the ageing of the bilayer assembly, PET substrate films were aged using the same conditions.

The mechanical and thermal properties of PET films both before and after 500h at 120°C are summarized in **Table 3**. The Young's modulus, the strain at break and the melting temperature (T_m) remained unchanged after thermal ageing. PET crystallinity increased slightly, presumably as a result of thermal annealing.

Table 3. Changes in mechanical and thermal properties of PET films induced by the different ageing conditions

Ageing	*E (MPa)*	ε_B *(%)*	T_m	χ_c *(%)*
Reference	5049 ± 42	72.7 ± 5.7	258°C	28%
500h 120°C	5116 ± 289	71.0 ± 17.6	256°C	32%
F1	5212 ± 177	71.8 ± 2.1	257°C	35%
F2	5538 ± 42	74.4 ± 8.6	257°C	30%
TM1	4932 ± 250	61.1 ± 20.2	256°C	33%
TM2	4828 ± 312	72.0 ± 11.3	256°C	34%

The Raman spectra of the PET substrate before and after 500h at 120°C are presented in **Figure 7**. The initial spectrum exhibits the conventional vibration bands of PET [26,27]. There was no spectral modification after thermal ageing. Instead, a broad peak covering the entire scan range appeared. However, the chemical structure of the PET substrate film should not be modified by thermal ageing under these thermal ageing conditions. Thus, the observed peak broadening is probably due to the fluorescence that emanates from the adjacent PNE layer (see description in the next part).

After thermal ageing at 120°C for 500h, the chemical structure and mechanical properties of the PET substrate films were conserved. The parameter change of note was an increase in PET crystallinity, possibly due to the annealing process.

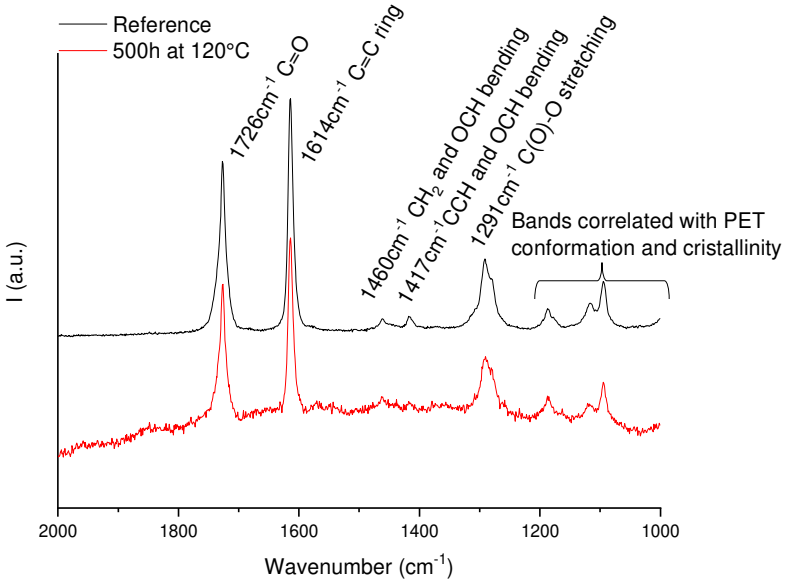

Figure 7. Raman spectra of PET substrate TV before (Reference) and after thermal ageing at 120°C for 500h

3.2.3. Bilayer and test vehicle ageing

PET/PNE bilayer systems and TV were all thermally aged under the same conditions. The bilayer systems were employed to characterize thermal ageing on the interface quality between encapsulant and substrate. TVs were used to determine the effects of thermal ageing on their functional properties (*i.e.* electrical properties).

The results of the peeling tests performed on bilayer systems are presented in **Table 4**. An adhesive rupture was observed both before and after ageing. The value of the peeling force G increased after thermal ageing at 120°C for 500h. The changes observed followed the same trend as both the Tg and mechanical properties of the epoxy resin while the substrate properties remained unchanged. The crosslinking reactions

occurring in the epoxy resin during thermal ageing led to an increased peeling strength, although the exact mechanism that underlies this phenomenon remains unclear. Accordingly, complementary experiments are needed to decipher this mechanism and those will be the subject of a separate study.

Table 4. Changes in the peeling force between PET and PNE films induced by the different ageing conditions

Ageing	*G (N/cm)*	*ΔG (N/cm)*	*Rupture*
Reference	1.74	0.15	Adhesive
500h 120°C	2.70	0.14	Adhesive
F1	1.63	0.11	Adhesive
F2	1.72	0.05	Adhesive
TM1	2.61	0.19	Adhesive
TM2	2.50	0.16	Adhesive

Both unaged and thermally aged TV successfully passed the electrical test (**Table 5**).

After thermal ageing, the epoxy resin deposited on TV presented marked yellowing (**Figure 8**), whereas the PET substrate was unchanged. Similar results were obtained after free films ageing.

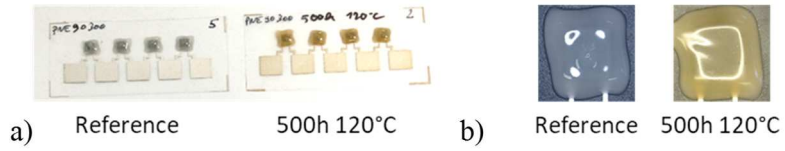

Figure 8. (a) Photographic image of a TV and (b) optical micrograph of on encapsulated chip before (Reference) and after thermal ageing (500h 120°C)

Confocal Raman spectroscopy was relied upon for the depth profiles needed to identify aged-induced changes in the chemical structure of the polymers used in TV. The results are presented in **Figure 9**.

Two areas are distinguishable on the reference TV. Intense vibration bands attributed to the PET substrate were detected for depths from 0 to approximatively 100 µm. There were no identifiable vibration bands for depths over 100 µm. The Raman signal of the studied epoxy resin was very low compared to that of PET.

A broader vibration band for depths greater than 100 µm (*i.e.* in the epoxy resin area) for thermally aged TV was evident. This band presumably arises from fluorescent groups derived from the chemical degradation of the epoxy resin. Indeed, samples undergoing yellowing were also the ones that exhibited Raman spectra modified by fluorescence due to the thermal oxidation of the polymer. The yellowing of polymers during oxidative ageing has already been described [28–30]. Moreover, fluorescent oxidation products can form in polymer materials during oxidative ageing [31,32]. Accordingly, the fluorescence serves as an indicator of the formation of oxidation products during thermo-oxidative ageing. These results are verifiable through FTIR analytical results obtained on aged PNE films.

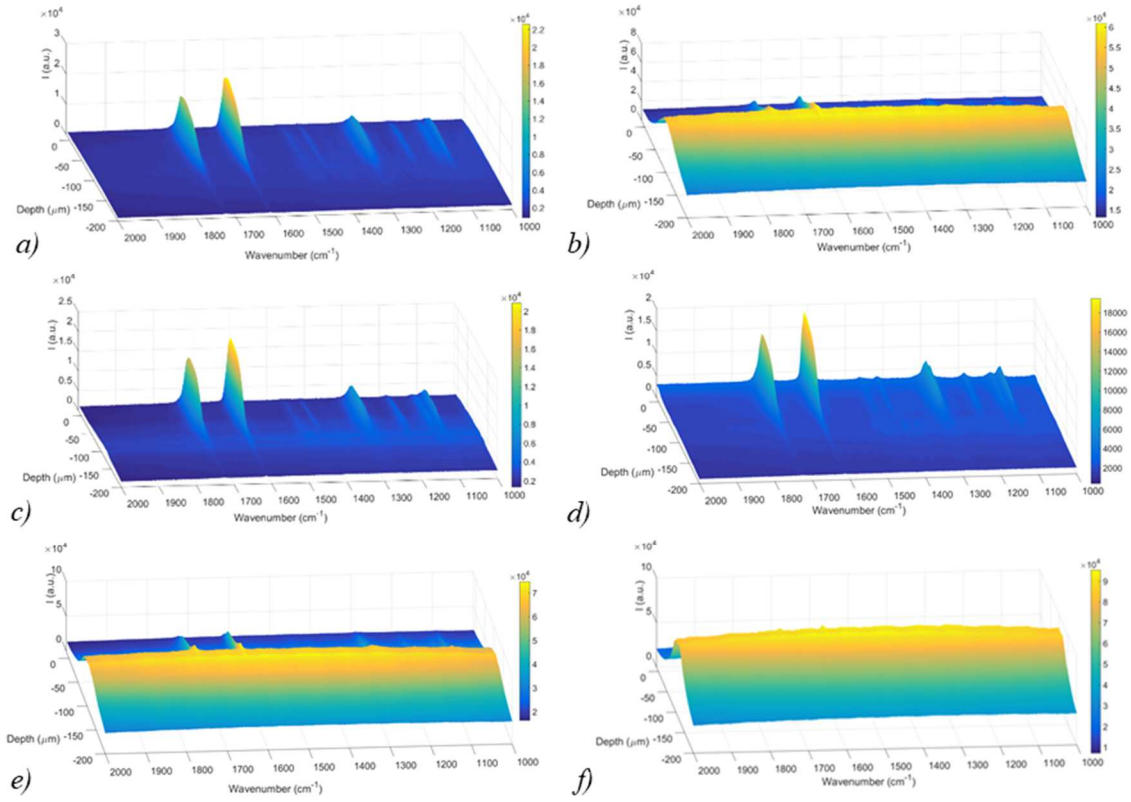

Figure 9. Raman depth profiles of TVs a) before; and after ageing under b) 500h, c) F1, d) F2, e) TM1 and f) TM2 conditions

A stiffening of the epoxy resin coupled with an increase in both T_g and T_d after thermal ageing at 120°C for 500h, were evidenced, as previously discussed. Such changes are associated with the dominance of crosslinking reactions. Changes in the epoxy chemical structure were apparent from the yellowing of the films and the formation of fluorescent oxidation products. Additionally, the PET substrate was shown to be stable, both from a chemical and mechanical perspective.

The force needed to peel the epoxy resin from the substrate increased due to the crosslinking reactions occurring during thermal ageing. TV functional properties were not affected by this reinforcement because the intensity of the increase was not sufficient.

3.3. Mechanical fatigue

3.3.1. Epoxy resin fatigue

The thermal and mechanical properties of the epoxy resins, following fatigue ageing under F2 conditions were determined using DMTA, tensile tests and TGA. The corresponding results are presented in **Table 2**.

The Young's modulus increased from a reference value 33 ± 1 MPa to 50 ± 6 MPa after fatigue ageing under F1 conditions, indicating a stiffening of the films. However, the stiffening recorded under F1 condition remained modest upon comparison, with the 133 ± 32 MPa recorded for thermal ageing at 120°C for 500h. Between F1 and F2 fatigue ageing conditions, PNE films stiffening increased further. Fatigue ageing under F2 conditions did not affect the glass transition (T_g), β-transition (T_β) or decomposition (T_d) temperatures. Additionally, the thermo-mechanical properties of PNE resin films were not significantly affected by fatigue at room temperature. In order to confirm these trends, fatigue experiments should be either continued under the same or harsher conditions.

3.3.2. PET substrate fatigue

The evolution of the PET substrate films properties subjected to mechanical fatigue appears in **Table 3**. After fatigue ageing, the PET Young's modulus increased reflecting a stiffening of the substrate. The crystallinity ratio was modified, whereas the melting temperature was unchanged.

Micro-Raman spectra, obtained for PET substrates before and after mechanical fatigue under F1 and F2 conditions, are presented in **Figure 10**. Raman spectra after fatigue testing at ambient temperature remained unchanged, suggesting that the PET chemical structure was stable under these conditions.

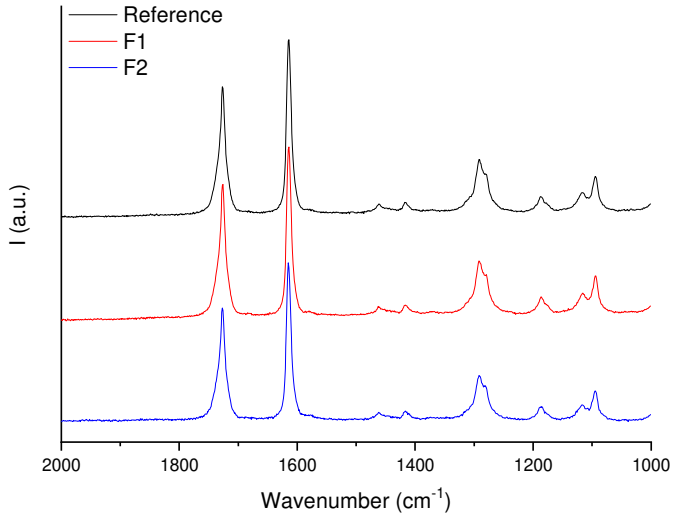

Figure 10. Changes in micro-Raman spectra of PET substrate in TVs before and after mechanical ageing under F1 and F2 conditions

The observed stiffening of PET after F1 is well explained by the increase in crystallinity in the polymer. However, the additional increase of stiffening, indicated by an increase in Young's modulus after F2, is nonetheless accompanied by a marked decrease in crystallinity back to its initial value. Another stiffening mechanism is involved in this case. The additional stiffening mechanism is presumably due to the presence of crosslinking reactions. For both F1 and F2 fatigue conditions, there was no sign of a modification of the chemical structure of PET. However, the chemical bond formed by the crosslinking reaction might not be active in Raman spectroscopy. Accordingly, complementary analyses are required to confirm the presence of crosslinking reactions.

3.3.3. Bilayer and test vehicle fatigue

The change in peeling force G between the PET substrate and PNE resin with fatigue ageing is reported in **Table 4**. The peeling force G remained stable after mechanical ageing, and adhesive ruptures were observed for each condition and each sample tested. The interface quality was unaffected under the fatigue conditions of the study.

TVs electrical testing after fatigue in condition F1 was positive. However, the tests were negative after condition F2 (**Table 5**), indicating a discontinuity in the electrical circuit. Under these harsher conditions, TV failure was observed even earlier, after 5 000 cycles on the 50 mm diameter roll followed by 3 000 additional cycles on the 25 mm diameter roll. Optical microscopy was performed on TVs to determine the origin of these failures. **Figure 11** presents a microscopic image of a chip on a TV that failed the electrical test. This micrograph was captured through the transparent PET substrate to examine the electrical circuit under the chip. For this micrograph, cracks (denoted as red lines) formed within the glue layer at the substrate and the chip interface, under the harshest condition during mechanical ageing. These cracks are probably due to the marked differences in stiffness between the silicon chip and the PET film. Under these conditions, stress accumulates in the glue layer leading to cracking.

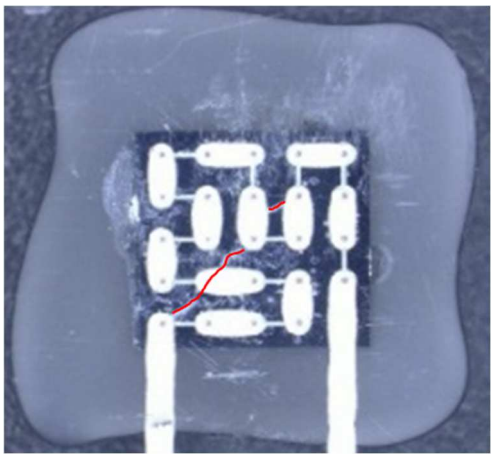

Figure 11. Optical micrograph of a TV after it was subjected to fatigue ageing under F2 conditions

The micro-Raman depth profile of TV subjected to fatigue under F1 and F2 conditions are presented in **Figure 9** c and d. These profiles indicate that TVs were unaffected by fatigue for both F1 and F2 conditions. The chemical structure of both substrate and encapsulant layer presented no detectable chemical modification.

After mechanical fatigue, the studied epoxy resin presented slight stiffening while its other properties remained unchanged. A stiffening of the PET substrate was similarly accompanied by increases in its crystallinity but with no change in its chemical structure. These microstructure modifications are probably due to mechanical effects only. The frequency of mechanical cycles used was probably too low to induce a substantial rise in the internal temperature by the friction of polymer macromolecules. The chemical structure of both PET and epoxy resin was also stable under these ageing conditions.

TV succumbed to electrical failure under the harshest ageing condition following the formation of cracks in the glue layer.

3.4. Thermo-mechanical coupling

All sample types were thermo-mechanical aged. Samples were first aged for 500h at 120°C under air, followed by mechanical bending for 5 000 cycles on a 50 mm diameter roll (TM1) and finally to 5 000 cycles on a 25 mm diameter roll (TM2). Mechanical bending cycle experiments were performed at ambient temperature. Samples characterization used the same techniques as previously described.

3.4.1. Epoxy resin TM coupling

Analytical characterization of PNE resin was by DMTA, tensile tests and TGA. The results are summarized in **Table 2**.

After ageing under condition TM1, T_g, T_d, and Young's modulus increased. T_β was unchanged. Visual inspection of the samples revealed a yellowing of the resin. The effect of thermo-mechanical ageing under TM1 condition was the combination of both thermal ageing for at 120°C for 500h and mechanical fatigue under F1 condition. As previously explained for thermal ageing, the simultaneous increase in these parameters reveals that crosslinking reactions were predominant. Based on the phenomenon of intensity difference between thermal ageing and mechanical fatigue as previously described, most of the changes observed under the combined regimen were due to thermal ageing. Yellowing of the resin observed after 500h at 120°C did not change during the subsequent fatigue.

Both T_g and Young's modulus decreased under the harshest (TM2) ageing conditions. An increase in the effectiveness of chain scission reactions explains this effect.

As for thermal ageing and fatigue, the β-transition was not affected by thermo-mechanical ageing under either condition.

A two steps system is identified as underpinning the thermo-mechanical ageing of epoxy resins. The first step TM1 is the direct addition of thermal ageing and fatigue F1. During this step, the crosslinking reactions proved dominant as evidenced by the stiffening of the films and increasing of their glass transition temperature. Yellowing of the resins due to thermal ageing was similarly recorded.

The second step TM2 presented different mechanisms, evidenced by a softening of the films and a decrease in T_g. During this step, chain scission reactions became more competitive.

3.4.2. PET substrate TM coupling

The changes in thermal and mechanical properties of PET substrates with thermo-mechanical ageing are presented in **Table 3**. The Young's modulus, strain at break and melting temperature for the PET substrate, after thermo-mechanical ageing, were not significantly modified under either condition. However, the PET substrate crystallinity ratio increased slightly. As for the recorded increase in crystallinity after thermal ageing, this is probably the result of a thermal annealing effect on the film.

The Raman spectra of PET films after thermo-mechanical ageing are presented in **Figure 12**. Both the peak positions and their width were unchanged after ageing, suggesting that the chemical structure of PET was stable during ageing under these conditions.

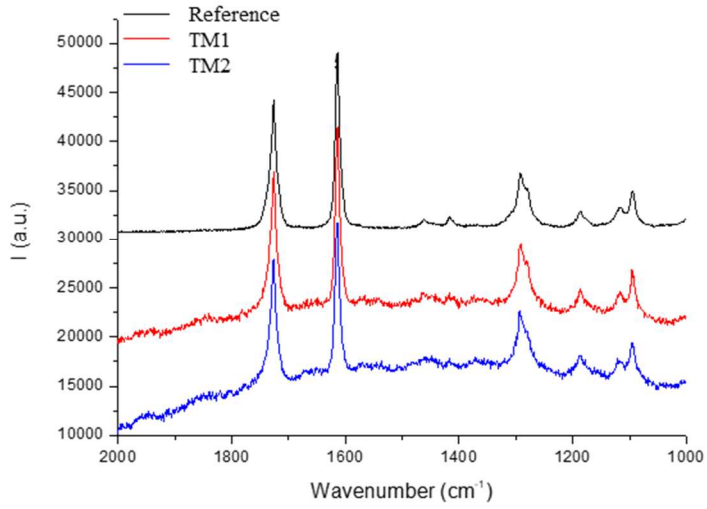

Figure 12. Changes in micro-Raman spectra of PET substrate in TVs before and after thermo-mechanical ageing under TM1 and TM2 conditions

Indeed, the mechanical, thermal and chemical properties of the PET films remained stable under thermo-mechanical ageing.

3.4.3. Bilayer and test vehicle TM coupling

The PET/PNE bilayer and TV were all subjected to thermo-mechanical ageing. The values of the peeling force G recorded after ageing are reported in **Table 4**. After ageing under TM1 conditions, the peeling force increased from 1.74 ± 0.15 N/cm to 2.61 ± 0.19 N/cm. However, this value is of the same magnitude as that recorded after thermal ageing at 120°C for 500h (2.70 ± 0.14 N/cm), suggests that the recorded increase during thermos-mechanical ageing TM1 was mainly due to the thermal ageing step. After ageing under condition TM2, a slight decrease in G was detected. This observation is consistent with the increase in chain-scission efficiency, evidenced for the epoxy resin ageing under this condition.

The results of the electrical tests performed on TV are presented in **Table 5**. These tests were positive for all the chips tested after thermo-mechanical ageing under both conditions. However, the TV aged under the harshest condition (TM2) presented some delamination between the PET substrate and the encapsulating resin.

Illustrated by the micrograph shown in **Figure 13**, delamination occurred on each side of the silicon chip and parallel to the bending direction. This is also explained by the stiffening of the resin measured after thermo-mechanical ageing. Thus conformability of the resin is reduced by this significant stiffening. Stresses then accumulate at the interface during the bending function of the TV. These observations are different from those observed for mechanical fatigue under F2 conditions. Here stresses are released when cracks form in the glue layer. Changes of both polymer materials during the thermo-mechanical ageing lead to modifications in the distribution of internal stresses that, in turn, results in different release modes.

Delamination between resin and substrate enabled water and oxygen to diffuse into the system. Accordingly, the encapsulation layer ceases to play its protective role. Functional properties would be degraded with longer ageing periods.

Table 5. Results of electrical tests performed on TV devices after each ageing condition

Ageing type		**Thermal**	**Fatigue**		**Thermo-mechanical**	
Ageing condition	Reference	500h	F1	F2	TM1	TM2
Electrical test	Positive	Positive	Positive	Negative	Positive	Positive

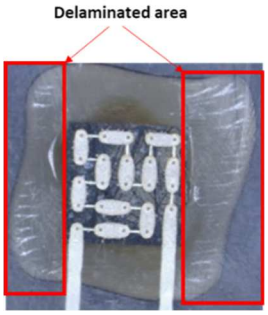

Figure 13. Optical micrograph of a TV after it was subjected to thermo-mechanically ageing under TM2 conditions

Micro-Raman depth profiles of TVs, that were thermo-mechanically aged, are presented in **Figure 9** e and f. As observed after thermal ageing, the micro-Raman depth profiles are dominated by a broad peak for depths greater than 100 µm when TVs were thermo-mechanically aged. Attributed to the formation of fluorescent species during thermo-oxidative processes, this peak was nevertheless not modified between TM1 and TM2 conditions.

Although yellowing of the epoxy resin developed during the thermal ageing stage, there was no recorded change during the subsequent mechanical ageing stage.

Conclusion

The durability and functional performances of microelectronic test vehicles comprising epoxy resin encapsulant and PET substrates have been thoroughly assessed after thermal, mechanical fatigue and thermo-mechanical ageing. Under moderate (TM1) ageing conditions, the changes observed resulted directly from combined thermal ageing and mechanical fatigue. Under these ageing conditions, oxidation of the epoxy resin resulting from the thermal ageing coupled with a stiffening of the films induces an increase of the peeling force, and reinforcement of the encapsulant/substrate interface. Whereas crosslinking reactions dominated under moderate ageing TM1 conditions, no further oxidation was detected under harsher TM2 conditions. Instead, chain scission reactions induced by fatigue stress following thermal ageing (TM2) were dominant. A softening of the epoxy resin coupled with a decrease in T_g was evidenced. The peeling force required to decouple the encapsulant from the substrate decreased, and delamination between the encapsulant and the substrate was observed in TV. While delamination does not always necessarily cause electrical failure, it probably induces damage to the barrier properties.

The peeling tests show that adhesion between the encapsulant and substrate is governed by degradation mechanisms occurring within the epoxy resin. The failure mechanism of TV as delamination or cracks in the glue layer is influenced by mechanical changes of all the constituting materials.

To that end, if the thermo-mechanical ageing remains inadequately controlled, a variety of reliability issues, circuit failure, performance degradation, ultimately leading to possible devices damage, will be the results.

Funding: This work was supported by Région Centre-Val de Loire through Regional project APR2015.

Acknowledgement: The authors would like to thank STMicroelectronics and Protavic International, the technical platforms of CERTeM located in Tours and of the IUT located in Blois.

Conflicts of Interest: The authors declare no conflict of interest.

References

1. N. Münzenrieder, G. Cantarella, C. Vogt, L. Petti, L. Büthe, G.A. Salvatore, Y. Fang, R. Andri, Y. Lam, R. Libanori, D. Widner, A.R. Studart, G. Tröster, Stretchable and Conformable Oxide Thin-Film Electronics, Adv. Electron. Mater. 1 (2015) n/a-n/a. https://doi.org/10.1002/aelm.201400038.
2. R. Carta, P. Jourand, B. Hermans, J. Thoné, D. Brosteaux, T. Vervust, F. Bossuyt, F. Axisa, J. Vanfleteren, R. Puers, Design and implementation of advanced systems in a flexible-stretchable technology for biomedical applications, EUROSENSORS XXII 2008. 156 (2009) 79–87. https://doi.org/10.1016/j.sna.2009.03.012.
3. Y.S. Rim, S.-H. Bae, H. Chen, N.D. Marco, Y. Yang, Recent Progress in Materials and Devices toward Printable and Flexible Sensors, Adv. Mater. 28 (2016) 4415–4440. https://doi.org/10.1002/adma.201505118.
4. V. Zardetto, T.M. Brown, A. Reale, A. Di Carlo, Substrates for flexible electronics: A practical investigation on the electrical, film flexibility, optical, temperature, and solvent resistance properties, J. Polym. Sci. Part B Polym. Phys. 49 (2011) 638–648. https://doi.org/10.1002/polb.22227.
5. W.A. MacDonald, M.K. Looney, D. MacKerron, R. Eveson, R. Adam, K. Hashimoto, K. Rakos, Latest advances in substrates for flexible electronics, J. Soc. Inf. Disp. 15 (2012) 1075–1083. https://doi.org/10.1889/1.2825093.
6. M. Gonzalez, B. Vandevelde, W. Christiaens, Y.-Y. Hsu, F. Iker, F. Bossuyt, J. Vanfleteren, O. van der Sluis, P.H.M. Timmermans, Design and implementation of flexible and stretchable systems, Therm. Mech. Multi-Phys. Simul. Exp. Micro-Electron. Micro-Syst. EuroSimE 2010. 51 (2011) 1069–1076. https://doi.org/10.1016/j.microrel.2011.03.012.
7. A. Salem, H. B. Akkerman, P. van de Weijer, P. C. P. Bouten, J. Shen, S. H. P. M. de Winter, P. Kudlacek, P. Panditha, H. Fledderus, J. J. van Glabbeek, L. M. Toonen, W. H. Manders, P. W. A. Groen, P. Poodt, M. Anderson, B. Gburek, Thin-film flexible barriers for PV applications and OLED lighting, in: 2016 IEEE 43rd Photovolt. Spec. Conf. PVSC, 2016: pp. 1661–1663. https://doi.org/10.1109/PVSC.2016.7749905.
8. J. Lewis, Material challenge for flexible organic devices, Mater. Today. 9 (2006) 38–45. https://doi.org/10.1016/S1369-7021(06)71446-8.
9. J. Gaume, C. Taviot-Gueho, S. Cros, A. Rivaton, S. Thérias, J.-L. Gardette, Optimization of PVA clay nanocomposite for ultra-barrier multilayer encapsulation of organic solar cells, 9th Int. Meet. Electrochromism. 99 (2012) 240–249. https://doi.org/10.1016/j.solmat.2011.12.005.
10. I. Topolniak, A. Chapel, J. Gaume, P.-O. Bussiere, G. Chadeyron, J.-L. Gardette, S. Therias, Applications of polymer nanocomposites as encapsulants for solar cells and LEDs: Impact of photodegradation on barrier and optical properties, Modif. Degrad. Stabilisation Polym. Concepts Appl. MoDeSt 2016. 145 (2017) 52–59. https://doi.org/10.1016/j.polymdegradstab.2017.06.013.
11. F. Bossuyt, J. Guenther, T. Löher, M. Seckel, T. Sterken, J. de Vries, Cyclic endurance reliability of stretchable electronic substrates, Microelectron. Reliab. 51 (2011) 628–635. https://doi.org/10.1016/j.microrel.2010.09.032.
12. E. Ernault, E. Richaud, B. Fayolle, Origin of epoxies embrittlement during oxidative ageing, Polym. Test. 63 (2017) 448–454. https://doi.org/10.1016/j.polymertesting.2017.09.004.
13. E. Ernault, E. Richaud, B. Fayolle, Thermal-oxidation of epoxy/amine followed by glass transition temperature changes, Polym. Degrad. Stab. 138 (2017) 82–90. https://doi.org/10.1016/j.polymdegradstab.2017.02.013.
14. F. Delor-Jestin, D. Drouin, P.-Y. Cheval, J. Lacoste, Thermal and photochemical ageing of epoxy resin – Influence of curing agents, Polym. Degrad. Stab. 91 (2006) 1247–1255. https://doi.org/10.1016/j.polymdegradstab.2005.09.009.

15. S. Bondzic, J. Hodgkin, J. Krstina, J. Mardel, Chemistry of thermal ageing in aerospace epoxy composites, J. Appl. Polym. Sci. 100 (2006) 2210–2219. https://doi.org/10.1002/app.23692.
16. L. Heux, J.L. Halary, F. Lauprêtre, L. Monnerie, Dynamic mechanical and 13C n.m.r. investigations of molecular motions involved in the β relaxation of epoxy networks based on DGEBA and aliphatic amines, Polymer. 38 (1997) 1767–1778. https://doi.org/10.1016/S0032-3861(96)00694-5.
17. A. Dupuis, F.-X. Perrin, A. Ulloa Torres, J.-P. Habas, L. Belec, J.-F. Chailan, Photo-oxidative degradation behavior of linseed oil based epoxy resin, Polym. Degrad. Stab. 135 (2017) 73–84. https://doi.org/10.1016/j.polymdegradstab.2016.11.021.
18. J. Brandrup, E.H. Immergut, E.A. Grulke, A. Abe, D.R. Bloch, Polymer handbook, Wiley New York etc, 1989.
19. A. Udagawa, Y. Yamamoto, Y. Inoue, R. Chûjô, Dynamic mechanical properties of cycloaliphatic epoxy resins cured by ultra-violet- and heat-initiated cationic polymerizations, Polymer. 32 (1991) 2779–2784. https://doi.org/10.1016/0032-3861(91)90108-U.
20. S. Morlat-Therias, E. Fanton, J.-L. Gardette, S. Peeterbroeck, M. Alexandre, P. Dubois, Polymer/carbon nanotube nanocomposites: Influence of carbon nanotubes on EVA photodegradation, Polym. Degrad. Stab. 92 (2007) 1873–1882. https://doi.org/10.1016/j.polymdegradstab.2007.06.021.
21. D.J. Carlsson, R. Brousseau, C. Zhang, D.M. Wiles, Identification of Products from Polyolefin Oxidation by Derivatization Reactions, in: Chem. React. Polym., American Chemical Society, 1988: pp. 376–389. https://doi.org/10.1021/bk-1988-0364.ch027.
22. C. Wilhelm, J. Gardette, Infrared identification of carboxylic acids formed in polymer photooxidation, J. Appl. Polym. Sci. 51 (1994) 1411–1420. https://doi.org/10.1002/app.1994.070510808.
23. O. Sindt, J. Perez, J.F. Gerard, Molecular architecture-mechanical behaviour relationships in epoxy networks, Polymer. 37 (1996) 2989–2997. https://doi.org/10.1016/0032-3861(96)89396-7.
24. N. Rasoldier, X. Colin, J. Verdu, M. Bocquet, L. Olivier, L. Chocinski-Arnault, M.C. Lafarie-Frenot, Model systems for thermo-oxidised epoxy composite matrices, Compos. Part Appl. Sci. Manuf. 39 (2008) 1522–1529. https://doi.org/10.1016/j.compositesa.2008.05.016.
25. S.R. Patel, S.W. Case, Durability of hygrothermally aged graphite/epoxy woven composite under combined hygrothermal conditions, Int. J. Fatigue. 24 (2002) 1295–1301. https://doi.org/10.1016/S0142-1123(02)00044-0.
26. Chiao-Chi Lin, Peter J. Krommenhoek, Stephanie S. Watson, Xiaohong Gu, Chemical depth profiling of photovoltaic backsheets after accelerated laboratory weathering, in: 2014: pp. 91790R-9179–12. https://doi.org/10.1117/12.2066400.
27. E. Rebollar, S. Pérez, M. Hernández, C. Domingo, M. Martín, T.A. Ezquerra, J.P. García-Ruiz, M. Castillejo, Physicochemical modifications accompanying UV laser induced surface structures on poly(ethylene terephthalate) and their effect on adhesion of mesenchymal cells, Phys. Chem. Chem. Phys. 16 (2014) 17551–17559. https://doi.org/10.1039/C4CP02434F.
28. S. Yang, S.-Y. Kwak, J. Jin, J.-S. Kim, Y. Choi, K.-W. Paik, B.-S. Bae, Thermally resistant UV-curable epoxy–siloxane hybrid materials for light emitting diode (LED) encapsulation, J. Mater. Chem. 22 (2012) 8874–8880. https://doi.org/10.1039/C2JM16355A.
29. N. S. Allen, M. Edge, M. Rodriguez, C. M. Liauw, E. Fontan, Aspects of the thermal oxidation, yellowing and stabilisation of ethylene vinyl acetate copolymer, Polym. Degrad. Stab. 71 (2000) 1–14. https://doi.org/10.1016/S0141-3910(00)00111-7.
30. J.-L. Gardette, Fundamental and technical aspects of the photooxidation of polymers, Environ. Sci. Pollut. CONTROL Ser. (2000) 671–698.
31. C. Peike, T. Kaltenbach, K. A. Weiß, M. Koehl, Indoor vs. outdoor aging: polymer degradation in PV modules investigated by Raman spectroscopy, in: 2012: pp. 84720V-8472–8. https://doi.org/10.1117/12.929828.
32. N.S. Allen, M.J. Harrison, G.W. Follows, V. Matthews, Thermal and photo-chemical degradation of nylon 6,6 polymer: Part 1—Influence of amine-carboxyl end group balance on luminescent species, Polym. Degrad. Stab. 19 (1987) 77–95. https://doi.org/10.1016/0141-3910(87)90014-0.